Supplementary Information

Stephen J. Royle, Nicholas A. Bright & Leon Lagnado "Clathrin is required for the function of the mitotic spindle"

Changes in the distribution of clathrin during the cell cycle

The subcellular distribution of clathrin in NRK cells depended on the phase of the cell cycle[1-4], as shown in Supplementary Fig. S1a. During interphase, GFP-tagged clathrin light chain a (GFP-LCa) was associated with the Golgi apparatus and numerous puncta representing clathrin-coated pits and vesicles[5]. Clathrin remained associated with the Golgi apparatus as it surrounded the nucleus at prophase[6], but began to localise with microtubules invading the nuclear space during prometaphase (Supplementary Fig. S1a). The association between clathrin and filamentous microtubules forming the spindle array was particularly obvious at metaphase. Clathrin appeared to localise to kinetochore fibres and possibly interpolar microtubules, but not astral microtubules of the spindle apparatus[7]. Clathrin remained co-localised with α-tubulin until late anaphase, but during telophase clathrin puncta again became predominant throughout the cell (Supplementary Fig. S1a). Similar changes in the distribution of clathrin were observed using other variants of the light chain tagged by GFP or by immunocytochemistry using a monoclonal antibody specific for the heavy chain (Supplementary Figs. S2,S3).

Clathrin at the mitotic spindle could be labelled with GFP-LCa, GFP-nLCa or GFP-LCb.

There are two variants of clathrin light chain, LCa and LCb. Each variant also has a neuron-specific isoform, nLCa and nLCb[8]. GFP-LCa, GFP-nLCa and GFP-LCb were each found together with clathrin heavy chain (CHC) at the mitotic spindle of NRK cells (Supplementary Fig. S2). This suggests that the targeting of clathrin was independent of the light chain and was determined by the heavy chain. In the main paper we show that the localisation of clathrin to the mitotic spindle depends on the heavy chain (Fig. 2).

Clathrin remained bound to the mitotic spindle after removal of soluble proteins.

We extracted soluble proteins from NRK cells without disrupting the cytoskeleton by incubating in BRB80 with 1 % Triton X-100 for 5 min at 37 °C prior to fixation (Supplementary Fig. S3). This treatment removes proteins that are not bound to the cytoskeleton[9], but did not result in loss of clathrin at the mitotic spindle. This result indicates that clathrin is bound to the spindle apparatus in living cells. Detergent-extraction of proteins from cells at interphase caused a loss of diffuse clathrin immunoreactivity but larger clathrin puncta (representing clathrin coated pits and vesicles) remained[5].

Clathrin at the mitotic spindle was associated with microtubules but not vesicles

Was clathrin bound to the mitotic spindle or did it localise as a store of CCVs? Clathrin does not bind membranes directly; the clathrin coat is formed by the binding of triskelia to adaptor proteins which recognise cargo proteins in the membrane[10]. The major adaptor proteins are AP-1, AP-2 and AP-3[11,12]. In cells at interphase, the great majority of clathrin puncta were labelled by antibodies that recognise AP-1 and AP-2, and the Golgi apparatus was labelled by antibodies against AP-1 and AP-3 (Supplementary Fig. S4a-c). But in cells at metaphase, none of these adaptors were associated with clathrin at the spindle apparatus (Supplementary Fig. S4a-c). Rather, clathrin-coated structures containing AP-2 were ‘arrested’ at the plasma membrane, consistent with inhibition of CME during mitosis[13].

Depletion of clathrin heavy chain by RNAi

RNA interference (RNAi) was used to knockdown the expression of CHC. We used two different strategies:

1. Transfection of short interfering RNA (siRNA) specific for rat CHC, usually in combination with a fluorescent marker (GFP or GFP-tagged protein); using a rat cell line (NRK cells).

2. Expression of short hairpin RNA (shRNA) specific for human CHC together with a fluorescent marker from the same plasmid, pBrain (see Methods); using a human cell line (HEK293 cells).

We were therefore able to test whether the mitotic defects caused by depletion of clathrin were specific to one cell type. The results from experiments with the human cell line were very similar to those described for the rat cell line (see Supplementary Table S1 for a comparison). Knockdown of CHC by transfection of siRNA has been demonstrated previously in human HeLa cells[14,15].

Treatment of NRK cells with siRNA reduced CHC to ~10 % of controls and this effect was maximal at 72 h post-transfection (Supplementary Fig. S5a, b). Depletion of CHC also inhibited CME; uptake of transferrin was markedly reduced during 5, 15 or 30 minute incubations at 37 °C (Supplementary Fig. S5c, d). In agreement with earlier studies[14,15], depletion of clathrin resulted in fewer cells per unit area (Supplementary Fig. S5e) and that this was not attributable to increased cell death. Dead or dying cells, as judged by nuclear morphology, only accounted for 0.26 % of all counted cells (compared to 0.07% in controls). Depletion of clathrin also increased the incidence of cells with multiple nuclei[14]to 6.8 ± 1.2 % of the total number of cells in interphase, compared to 0.5 ± 0.2 % in controls.

We are uncertain how far clathrin may be involved in cytokinesis in mammalian cells. Cytokinesis is impaired in clathrin-null *Dictyostelium* cells in suspension[16], leading to the idea that clathrin is involved in membrane trafficking during cell division[17]. However, cytokinesis can occur in clathrin-null *Dictyostelium* cells attached to a substrate[18]. We only saw a modest increase in the number of multinucleate cells after CHC RNAi. In addition, we did not find clathrin localised to the midbody (Supplementary Fig. S1a)[18] where proteins involved in cytokinesis, such as dynamin, are found[19].

The major difference between mitotic defects in rat and human cell lines was the higher frequency of misaligned chromosomes in the human cell line after depletion of clathrin

(Supplementary Table S1). An overview of experiments carried out in rat and human cell lines is shown in Supplementary Table S2.

Depletion of clathrin did not significantly alter spindle morphology

Depletion of clathrin did not significantly alter the structure of the spindle (Supplementary Fig. S6). In contrast, mitotic spindles are extremely disorganised when RNAi is used to deplete other proteins associated with the spindle, such as NuSAP[20] or ch-TOG[21]. Clathrin was not, therefore, essential for assembly or maintenance of the mitotic spindle.

Further mitotic defects in cells depleted of clathrin

Lagging chromosomes at anaphase and telophase. Misaligned chromosomes were found at metaphase (Fig. 4, main paper), and lagging chromosomes were also found at anaphase and telophase in some cells depleted of clathrin. Supplementary Fig. S7a shows an example of a cell in telophase with a chromosome "stranded" between the two daughter nuclei. These chromosomes were composed of sister chromatids, as shown by the double-dot staining of CENP-B (Lower panel of Supplementary Fig. S7a), and they were therefore not segregated during anaphase.

Persistent checkpoint signalling. Fig. 4 of the main paper shows that GFP-hMad2 localised to kinetochores of misaligned chromosomes as well as chromosomes at the metaphase plate in cells depleted of clathrin. We obtained similar results with a polyclonal antibody directed against Mad2 (Supplementary Fig. S7b,c). In cells expressing CHC shRNA, Mad2 immunoreactivity was localised to a subset of CENP-B-positive centromeres of chromosomes that were bi-oriented at the metaphase plate and those that were misaligned. The high, particulate background staining of this antibody was problematic and prompted us to confirm these results with GFP-hMad2 (see main paper).

Methods

Molecular biology

DNA constructs. GFP-LCa, GFP-nLCa and GFP-LCb were generated by PCR to introduce *Bgl* II and *Eco*R I sites and were subcloned into pEGFP-C1 (Clontech). GFP-CHC(1-479), GFP-CHC(1-330) and GFP-CHC(331-1074) were amplified and subcloned into *Bgl* II and *Hin*d III sites of pEGFP-C1 and GFP-CHC(1-1074) was made by subcloning a *Bgl* II-*Sca* I fragment from GFP-CHC(1-479) into GFP-CHC(331-1074). In addition, GFP-CHC(1-479) was rendered knockdown-proof by silent mutations in the CHC shRNA binding region using the megaprimer method (TCCAATTCGAAGACCAAT to TCCgATcaGgcGtCCtAT) to give GFP-CHC(1-479)KDP. Knockdown-proof GFP-CHC(1-1639) was made by subcloning an *Age* I-*Mfe* I fragment of CHC(1-1639) into pEGFP-C1 at *Xma* I-*Mfe* I sites and then repairing the N-terminus by substituting a *Bgl* II-*Asp*718 fragment from GFP-CHC(1-479)KDP. GFP-tagged histone 2B (H2B-GFP), was made by amplifying H2BK to introduce a *Kpn* I site and Kozak initiation sequence at the 5' end and to remove the stop codon and add a *Bam*H I site to the 3' end, the digested fragment was ligated into pEGFP-N1 at *Kpn* I-*Bam*H I sites. GFP-hMad2 was reconstructed to enable us to make pBrain versions (see below). GFP-hMad2 in pCS2 was amplified to introduce *Bgl* II and *Hin*d III sites and the resulting fragment was cloned into pEGFP-C1.

All constructs used in this study were verified by automated DNA sequencing (Lark, UK or MRC Geneservice, UK). Sequences of all primers used are available on request.

Complementary DNAs. Human CHC (major splice variant, residues 1-1639) and clathrin light chains LCa and LCb, H2BK cDNAs (I.M.A.G.E. 6187185, 3944942, 4299637 and 6093977) were purchased from MRC Geneservice, Cambridge, UK. Human neuronal clathrin light chain nLCa cDNA in λgt10 (Accession: NM_007096)[22], was a kind gift from Dr. A. P. Jackson (Department of Biochemistry, Cambridge, UK). GFP-tagged α-tubulin was from Clontech (pEGFP-Tub). GFP-hMad2 in pCS2[23] was a kind gift from Dr G. Fang (Stanford University, USA).

Design of siRNAs and shRNAs. CHC siRNA was designed to target rat CHC[24] (Accession no. J03583, AATCGCCCTTCTGAAGGTCCT), according to the rules of Tuschl and colleagues[25,26]. Control siRNA was a scrambled version of the CHC siRNA (AATTCGCACCCTACTTCGTGG). Duplex siRNA was synthesised with dTdT overhangs with the 'crude scale' option (Qiagen). Both sequences were subject to a BLAST search to ensure that CHC siRNA was specific and that the control siRNA did not match any sequence. Oligonucleotides for expression of control (CHC1) or CHC (CHC4) shRNA are shown in Supplementary Table S3. CHC1 was designed against rat CHC (1817-1835 of NM_019299.1) and did not affect CHC expression in human cells due to a base change in this region of the mRNA (1931-1949 of BC051800.2, 1937 is A and also 1929 is T). CHC4 was designed against human CHC (391-409 of BC051800.2) according to Motley and colleagues[14].

Vectors for co-expression of shRNA and tagged proteins: pBrain. We made a series of vectors called pBrain that were similar to the pKoen vector made by Deneka and colleagues[27]. These vectors allowed the simultaneous expression of shRNA under an H1 RNA promoter and fluorescent proteins under a CMV promoter. Briefly, the H1 RNA promoter from pSUPER[28] was excised using *Pvu* II and was ligated into the filled-in *Ase* I site of a vector containing synaptopHluorin in the place of GFP in pEGFP-C1. Annealed oligos could be phosphorylated and inserted at the *Bgl* II/*Hin*d III site downstream of the H1 RNA promoter. The region containing the H1 RNA promoter together with the insert to make shRNAs could then be put into other pEGFP-C1- or pEGFP-N1-based vectors by exchanging an *Apa*L I-*Nhe* I fragment, for example.

The vector to co-express GFP and control shRNA was designated pBrain-GFP-CHC1 and the CHC RNAi vector was pBrain-GFP-CHC4. Each were made by ligating the *Apa*L I-*Nhe* I fragments from pBrain-SpH-CHC1 or -CHC4 into pEGFP-C1. To co-express GFP-tagged α-tubulin and shRNA, pBrain-GFP-Tub-CHC1 or -CHC4 were made by ligating the *Bgl* II-*Bam*H I fragment from pEGFP-Tub into the *Bgl* II site of pBrain-GFP-CHC1 or -CHC4. To co-express H2B-GFP and shRNA, pBrain-H2B-GFP-CHC1 or -CHC4 were made by ligation of *Apa*L I-*Nhe* I fragments from pBrain-SpH-CHC1 or -CHC4. To express GFP-hMad2 and

shRNA the hMad2 fragment was ligated into pBrain-GFP-CHC1 and -CHC4 at *Bgl* II and *Mlu* I (due to an *Apa*L I site in hMad2) to give pBrain-GFP-hMad2-CHC1 and -CHC4. Following recent work[29], we only examined GFP-hMad2 expressing cells that were fluorescing extremely weakly. To co-express GFP-CHC(1-479)KDP and shRNA, an *Apa*L I-*Age* I fragment from pBrain-GFP-CHC1 or -CHC4 was ligated into GFP-CHC(1-479)KDP. To co-express GFP-CHC(1-1639)KDP and CHC shRNA, a *Bgl* II-*Mfe* I fragment from GFP-CHC(1-1639)KDP was ligated into pBrain-GFP-CHC4. For expression of GFP-CHC(1-1639)KDP without knockdown of endogenous clathrin, GFP-CHC(1-1639)KDP was used without expression of control shRNA. When using pBrain vectors, we found a weak negative correlation between the amount of fluorescence (protein expression) and the degree of knockdown (shRNA expression), presumably reflecting competition for translation. We saw the weakest knockdown with the brightest cells and so analysis was confined to weakly expressing cells to ensure good knockdown. Of all the CHC4 pBrain vectors we made, pBrain-H2B-GFP-CHC4 performed the worst; this was probably due to the unusually strong expression of H2B-GFP.

Cell culture

Maintenance of cell lines. Normal rat kidney (NRK) cells (kind gift from Dr G. Ihrke, Cambridge Institute for Medical Research, UK) and human embryonic kidney (HEK293) cells were each maintained in DMEM containing 10 % fetal bovine serum (FBS) and 100 U/ml penicillin-streptomycin (pen-strep) at 37 °C and 5 % CO_2.

Transfection. NRK cells were transfected with DNA plasmids and/or siRNAs using Lipofectamine 2000 (Invitrogen) according to the manufacturer's instructions. For DNA/siRNA co-transfection experiments, we found that the method previously described[25] resulted in many knockdown cells, but very few cells transfected with DNA albeit with a high co-transfection rate. To circumvent this problem we prepared separate nucleic acid/liposome mixtures containing 50 % of the Lipofectamine 2000 and applied them both to the cells at the same time. This resulted in many more cells transfected with the marker plasmid, with a

similar high degree of co-transfection (~95 %). In a typical experiment 1 well of a six-well plate contained 2 cover slips and 2 ml medium without antibiotics, 3 µg DNA were diluted in 50 µl DMEM, 12 µl siRNA (stock 40 µM) was diluted in 50 µl DMEM, to each of these 50 µl DMEM containing 2 µl Lipofectamine 2000 was added. 20 min later, 100 µl of each were added to 1 well. Complete medium (with antibiotics) was replaced after 6-8 h. For some experiments, confluent cells were transfected as above and were reseeded after 24 h in order to clearly image single cells.

HEK293 cells were plated on poly-L-lysine-coated cover slips at 50,000 cells/ml on the day before transfection. Cells were transfected with DNA plasmids using calcium phosphate precipitation as previously described[30].

Mitotic enrichment. Exponentially growing NRK cells were seeded into ten 75 cm^2 flasks at a density of ~1.8 million per flask. The following morning 1 ml of medium was exchanged for 1ml of medium containing 40 mM thymidine (2 mM final). Twelve hours later medium was aspirated, cells were washed with normal culture medium and the medium was replaced with 10 ml of medium supplemented with 70 ng/ml nocodazole. Twelve hours later the cells were washed and mitotic cells were removed by shake-off.

Immunocytochemistry

Immunostaining was performed as previously described[30]. The following monoclonal antibodies were used: anti-clathrin heavy chain and anti-α-adaptin (X22 and AP6, Affinity BioReagents), anti-α-tubulin and anti-β1/2-adaptin (DM1A and 100/1, Sigma), anti-CENP-B[31] was a kind gift from Prof. W. C. Earnshaw (University of Edinburgh, UK) and anti-δ-adaptin (clone SA4)[32] and polyclonal anti-δ-adaptin were kind gifts from Prof. M. S. Robinson (Cambridge Institute for Medical Research, U.K.). Polyclonal anti-Mad2 was from Covance. Rabbit polyclonal anti-clathrin antiserum was as previously described[33]. Goat anti-mouse or anti-rabbit Cy3-conjugated secondary antibodies were from Jackson ImmunoResearch and goat anti-mouse Alexa647 secondary antibodies were from Molecular Probes. Goat anti-mouse IgG conjugated to 10 nm colloidal gold was from Biocell. Protein A

conjugated to 15 nm colloidal gold was from Department of Cell Biology, University of Utrecht. TOPRO-3 (Molecular Probes) and Hoechst 33342 (Sigma) were used for staining DNA/RNA.

Transferrin uptake. Uptake of Transferrin-Alexa546 (Molecular Probes) was done as previously described[34]. Cells were incubated in serum-free DMEM for 15 min at 37 °C, then kept in serum-free DMEM containing 50 µg/ml transferrin-Alexa546 for 15 min at 37 °C. Cells were washed twice in PBS and then fixed and mounted for microscopy.

Membrane staining. FM4-64 (N-(3-Triethylammoniumpropyl)-4-(*p*-diethylaminophenylhexatrienyl)-pyridinium, 2Br) was from Calbiochem. For membrane-labelling experiments, transfected cells were cultured for >24 h in 15 µM FM4-64 at 37 °C, cells were washed for 5 min in imaging buffer (MEM without phenol red, 10% FBS, 100 U/ml pen-strep) before images were taken.

Extraction of soluble proteins. Detergent extraction experiments were done by incubating the cells first in PBS then in Brinkley reassembly buffer (BRB80, 80 mM Pipes/KOH, pH 6.8, 4 % polyethylene glycol 8000, 1 mM $MgCl_2$, 1 mM EGTA) containing 1% Triton X-100. Cells were washed once in BRB80 without Triton X-100, fixed, and processed for microscopy.

Imaging

Microscopy. Confocal imaging was done using a BioRad Radiance 2000 and Nikon TE300 microscope with 60x (1.4 NA) or 100x (1.3 NA) oil immersion objectives. GFP, Cy3 or FM4-64, and Alexa647 or TOPRO-3 were excited at 488, 543, and 633 nm, respectively. For double or triple labelling experiments, excitation and collection of emission were performed separately and sequentially. Power output of the primary laser was checked regularly to ensure consistency (50 ± 1 mW; anode current 7.1 ± 0.2 A). For quantitative immunostaining experiments, identical laser power and acquisition settings were used. Images were captured to Lasersharp 5.0 software at a depth of 8-bit. Analysis of single-cell immunoreactivity from greyscale images was carried out essentially as described previously[30,34]. Images were

imported into IMAGEJ (NIH) or IPLab 3.9 (Scanalytics) and the outline of the cell was manually drawn on the GFP channel of the image and then this ROI was transferred to the red channel and the mean pixel density was measured or the image was thresholded and the number of transferrin puncta were counted.

Spindle recruitment assay. Spindle recruitment was assayed by dividing the mean pixel density measured in a 1 μm x 1 μm ROI (10 x 10 pixel box) placed over the spindle ($F_{spindle}$) by that measured in a region outside the spindle ($F_{cytoplasm}$).

Metaphase plate thickness. The thickness of the metaphase plate was assessed by measuring the perpendicular distance between two limiting lines drawn parallel to the metaphase plate (see right panels of Fig. 5a, main paper).

Clathrin immunoreactivity at the mitotic spindle. To measure clathrin immunoreactivity at the mitotic spindle, each half-spindle was drawn around manually and the mean pixel density between the two areas was measured[21]. Note that endogenous clathrin could be detected separately from GFP-CHC(1-479) because monoclonal antibody X22 detects a region on the proximal leg of CHC[35,36].

Mitotic index. Experiments to determine the mitotic index were done by counting the number of cells with mitotic figures as a proportion of the total number of cells within a 275 x 190 μm area. Cells were counted if they were GFP-positive or, in the case of 72 h CHC RNAi, if they were depleted of clathrin (easily distinguished as those with ~10 % of the clathrin immunoreactivity of the surrounding cells). The number of metaphase-like cells that had misaligned chromosomes and the number of interphase cells that had multiple nuclei (defined as two or more nuclei or cells with one nucleus and one or more micronuclei) were counted. Cell death was quantified as the number of cells with pyknotic or blebbing nuclei as a fraction of the total number of cells. Cell density was the total number of nuclei (regardless of whether or not the cells were transfected) in a 275 x 190 μm area. This will give an underestimate of the decrease in cell density caused by CHC depletion, because faster dividing non-transfected cells will contribute to the cell density.

Measurement of interkinetochore distance. Cells were stained for CENP-B and imaged as described above. The distance between sister kinetochores found within the same confocal section were measured using IPLab. The distance reported by the computer was rounded to the nearest tenth of a micron.

Quantification and statistics. For image quantification and counting experiments, between 5-80 cells were analysed and 100-3914 cells were counted from experiments performed 3-6 times. Results were handled in Microsoft Excel version x (Microsoft) and in IGOR PRO 4.09A (Wavemetrics) and figures were assembled in Adobe Photoshop 7.0. Results are expressed as mean ± s.e.m. Unpaired Student's *t*-test was used to compare control versus test values and ANOVA with Dunnet's *post-hoc* test was used to compare multiple groups. Binomial results (mitotic index, misaligned chromosomes, multinucleate cells etc.) were tested for approximation to a normal distribution and *z*-values were calculated and *p*-values retrieved in Excel.

Immunoelectron microscopy Cells were prepared for ultrastructural analysis using immunogold EM as previously described[37]. Briefly, mitotic NRK cells were fixed with 4 % paraformaldehyde/0.1 % glutaraldehyde in 0.1 M sodium cacodylate, pH 7.2 at room temperature for 1 hour, infused with 1.7 M sucrose / 15 % poly-vinyl pyrolidone and prepared as previously described[37]. Ultrathin frozen sections were collected from the knife-edge with 50:50 2 % methyl cellulose:2.3 M sucrose[38] and immunolabelled, contrasted with methyl cellulose/uranyl acetate, dried and observed in a Philips CM100 TEM[37].

References

1. Louvard, D. et al. A monoclonal antibody to the heavy chain of clathrin. *EMBO J.* **2**, 1655-64 (1983).

2. Maro, B., Johnson, M. H., Pickering, S. J. & Louvard, D. Changes in the distribution of membranous organelles during mouse early development. *J. Embryol. Exp. Morphol.* **90**, 287-309 (1985).

3. Okamoto, C. T., McKinney, J. & Jeng, Y. Y. Clathrin in mitotic spindles. *Am. J. Physiol. Cell Physiol.* **279**, C369-74 (2000).

4. Sutherland, H. G. et al. Large-scale identification of mammalian proteins localized to nuclear sub-compartments. *Hum. Mol. Genet.* **10**, 1995-2011 (2001).

5. Gaidarov, I., Santini, F., Warren, R. A. & Keen, J. H. Spatial control of coated-pit dynamics in living cells. *Nat. Cell Biol.* **1**, 1-7 (1999).

6. Shorter, J. & Warren, G. Golgi architecture and inheritance. *Annu. Rev. Cell Dev. Biol.* **18**, 379-420 (2002).

7. Compton, D. A. Spindle assembly in animal cells. *Annu. Rev. Biochem.* **69**, 95-114 (2000).

8. Jackson, A. P., Seow, H. F., Holmes, N., Drickamer, K. & Parham, P. Clathrin light chains contain brain-specific insertion sequences and a region of homology with intermediate filaments. *Nature* **326**, 154-9 (1987).

9. Schell, M. J., Erneux, C. & Irvine, R. F. Inositol 1,4,5-trisphosphate 3-kinase A associates with F-actin and dendritic spines via its N terminus. *J. Biol. Chem.* **276**, 37537-46 (2001).

10. Kirchhausen, T. Clathrin. *Annu. Rev. Biochem.* **69**, 699-727 (2000).

11. Brodsky, F. M., Chen, C. Y., Knuehl, C., Towler, M. C. & Wakeham, D. E. Biological basket weaving: formation and function of clathrin-coated vesicles. *Annu. Rev. Cell Dev. Biol.* **17**, 517-68 (2001).

12. Robinson, M. S. Adaptable adaptors for coated vesicles. *Trends Cell Biol.* **14**, 167-74 (2004).

13. Warren, G. Membrane partitioning during cell division. *Annu. Rev. Biochem.* **62**, 323-48 (1993).

14. Motley, A., Bright, N. A., Seaman, M. N. & Robinson, M. S. Clathrin-mediated endocytosis in AP-2-depleted cells. *J. Cell Biol.* **162**, 909-18 (2003).

15. Hinrichsen, L., Harborth, J., Andrees, L., Weber, K. & Ungewickell, E. J. Effect of clathrin heavy chain- and alpha-adaptin-specific small inhibitory RNAs on endocytic accessory proteins and receptor trafficking in HeLa cells. *J. Biol. Chem.* **278**, 45160-70 (2003).

16. Niswonger, M. L. & O'Halloran, T. J. A novel role for clathrin in cytokinesis. *Proc. Natl. Acad. Sci. U.S.A.* **94**, 8575-8 (1997).

17. O'Halloran, T. J. Membrane traffic and cytokinesis. *Traffic* **1**, 921-6 (2000).

18. Gerald, N. J., Damer, C. K., O'Halloran, T. J. & De Lozanne, A. Cytokinesis failure in clathrin-minus cells is caused by cleavage furrow instability. *Cell Motil Cytoskeleton* **48**, 213-23 (2001).

19. Thompson, H. M., Skop, A. R., Euteneuer, U., Meyer, B. J. & McNiven, M. A. The large GTPase dynamin associates with the spindle midzone and is required for cytokinesis. *Curr. Biol.* **12**, 2111-7 (2002).

20. Raemaekers, T. et al. NuSAP, a novel microtubule-associated protein involved in mitotic spindle organization. *J. Cell Biol.* **162**, 1017-29 (2003).

21. Gergely, F., Draviam, V. M. & Raff, J. W. The ch-TOG/XMAP215 protein is essential for spindle pole organization in human somatic cells. *Genes Dev.* **17**, 336-41 (2003).

22. Jackson, A. P. & Parham, P. Structure of human clathrin light chains. Conservation of light chain polymorphism in three mammalian species. *J. Biol. Chem.* **263**, 16688-95 (1988).

23. Howell, B. J., Hoffman, D. B., Fang, G., Murray, A. W. & Salmon, E. D. Visualization of Mad2 dynamics at kinetochores, along spindle fibers, and at spindle poles in living cells. *J. Cell Biol.* **150**, 1233-50 (2000).

24. Kirchhausen, T. et al. Clathrin heavy chain: molecular cloning and complete primary structure. *Proc. Natl. Acad. Sci. U.S.A.* **84**, 8805-9 (1987).

25. Elbashir, S. M. et al. Duplexes of 21-nucleotide RNAs mediate RNA interference in cultured mammalian cells. *Nature* **411**, 494-8 (2001).

26. Elbashir, S. M., Harborth, J., Weber, K. & Tuschl, T. Analysis of gene function in somatic mammalian cells using small interfering RNAs. *Methods* **26**, 199-213 (2002).

27. Deneka, M. et al. Rabaptin-5alpha/rabaptin-4 serves as a linker between rab4 and gamma(1)-adaptin in membrane recycling from endosomes. *EMBO J.* **22**, 2645-57 (2003).

28. Brummelkamp, T. R., Bernards, R. & Agami, R. A system for stable expression of short interfering RNAs in mammalian cells. *Science* **296**, 550-3 (2002).

29. Howell, B. J. et al. Spindle checkpoint protein dynamics at kinetochores in living cells. *Curr. Biol.* **14**, 953-64 (2004).

30. Bobanovic, L. K., Royle, S. J. & Murrell-Lagnado, R. D. P2X receptor trafficking in neurons is subunit specific. *J. Neurosci.* **22**, 4814-24 (2002).

31. Earnshaw, W. C. et al. Molecular cloning of cDNA for CENP-B, the major human centromere autoantigen. *J. Cell Biol.* **104**, 817-29 (1987).

32. Peden, A. A. et al. Localization of the AP-3 adaptor complex defines a novel endosomal exit site for lysosomal membrane proteins. *J. Cell Biol.* **164**, 1065-76 (2004).

33. Simpson, F. et al. A novel adaptor-related protein complex. *J. Cell Biol.* **133**, 749-60 (1996).

34. Royle, S. J., Bobanovic, L. K. & Murrell-Lagnado, R. D. Identification of a non-canonical tyrosine-based endocytic motif in an ionotropic receptor. *J. Biol. Chem.* **277**, 35378-85 (2002).

35. Nathke, I. S. et al. Folding and trimerization of clathrin subunits at the triskelion hub. *Cell* **68**, 899-910 (1992).

36. Liu, S. H., Wong, M. L., Craik, C. S. & Brodsky, F. M. Regulation of clathrin assembly and trimerization defined using recombinant triskelion hubs. *Cell* **83**, 257-67 (1995).

37. Bright, N. A., Reaves, B. J., Mullock, B. M. & Luzio, J. P. Dense core lysosomes can fuse with late endosomes and are re-formed from the resultant hybrid organelles. *J. Cell Sci.* **110 (Pt 17)**, 2027-40 (1997).

38. Liou, W., Geuze, H. J. & Slot, J. W. Improving structural integrity of cryosections for immunogold labeling. *Histochem Cell Biol* **106**, 41-58 (1996).

Legends

Supplementary Figure S1 Clathrin was targeted to the mitotic spindle of NRK cells. Representative confocal micrographs showing the subcellular distribution of clathrin at each stage of mitosis. Left: GFP-LCa (green in overlay), centre: α-tubulin (red in overlay), right: overlay with nucleic acids in blue.

Supplementary Figure S2 Clathrin light chains were targeted to the mitotic spindle. GFP-tagged variants of light chain a (LCa), the neuronal isoform of light chain a (nLCa) and light chain b (LCb) were expressed in NRK cells and co-stained for CHC (using X22/Cy3, red). Example confocal micrographs for cells in interphase (above) or metaphase (below). Scale bar, 10 μm

Supplementary Figure S3 Clathrin remains associated with the spindle apparatus after extraction of soluble proteins. NRK cells in interphase (left) or metaphase (right) were fixed and stained for CHC (using X22/Cy3) following 5 min 37 °C incubation in PBS (control, above) or BRB80 containing Triton X-100 (extraction, below). Scale bar, 10 μm.

Supplementary Figure S4 The association of clathrin with microtubules was not via coated membranes. **a**, Representative micrographs of cells expressing GFP-LCa (left panels, green in overlay) co-stained for β1/2-adaptin (AP-1/AP-2, red in overlay), and nucleic acids (blue in overlay). The upper three panels show a cell in interphase and the lower three a cell at metaphase. Note that these adaptors were distributed in puncta throughout the cell at interphase, but these puncta were almost exclusively at the surface membrane in metaphase. **b**, A similar comparison in which cells were stained for α-adaptin (AP-2). AP-2 did not localise to the mitotic spindle. **c**, A similar comparison in which cells were stained for δ-adaptin (AP-3). Similar results were obtained using a polyclonal anti-δ-adaptin antibody. **d**, Example images of live cells imaged following a 24-28 h incubation with FM4-64 (red). Cells expressing either

GFP-α-tubulin (left panels, green) or GFP-LCa (right panels, green) are shown at interphase (above) or metaphase (below). Scale bars, 10 μm.

Supplementary Figure S5 Knockdown of clathrin heavy chain using RNAi. **a**, Example confocal images show co-transfection of GFP (green) together with control-siRNA (controls above) or CHC-siRNA (below). NRK Cells were co-stained for CHC (X22/Cy3). In the lower panels the green cell has much less CHC than its neighbours. Note that the transfection of siRNA is at higher efficiency than GFP (see Supplementary Methods). **b**, Quantification of cellular CHC levels. Histogram showing levels of CHC immunoreactivity in control NRK cells (open bars) and cells treated with CHC siRNA (black bars) 24, 48, and 72 h after transfection. Results normalised to the control value at each time point. **c**, Depletion of CHC caused an inhibition of CME, measured by transferrin uptake. Conditions for transfection are as described in **a**. Additionally, NRK cells were allowed to take up fluorescent transferrin (Transferrin-Alexa546) for 15 min at 37 °C. Note absence of fluorescent puncta and accumulation of fluorescent transferrin at the cell surface in cells depleted of CHC. Scale bar = 10 μm. **d**, Quantification of CME. Histogram to show number of fluorescent puncta taken up per confocal section after 5, 15, and 30 min incubation with Transferrin-Alexa546. Control NRK cells (open bars) and cells depleted of CHC (black bars) 72 h post-transfection. **e**, Depletion of CHC results in a lower density of NRK cells. Cell counts were performed on control cultures (open bars) or cultures transfected with CHC-siRNA (black bars), 72 h after transfection. NRK cells were seeded at an initial density of 0.7×10^5 cells/well. **f**, Histogram to show percentage of mitotic control or CHC RNAi HEK293 cells at each stage in mitosis. Values are mean ± s.e.m., ** $p < 0.01$, * $p < 0.05$.

Supplementary Figure S6 Clathrin depletion did not significantly alter spindle morphology. Two examples of cells transfected with control-siRNA and three examples of cells transfected with CHC-siRNA. Cells were co-transfected with GFP-α-tubulin (top, green in overlay) and stained for CHC (X22/Cy3, 2nd row, red in

overlay) and nucleic acids (TOPRO-3, 3rd row, blue in overlay). In cells depleted of clathrin, chromosomes were poorly aligned at the metaphase plate but there were no gross changes in the structure of the mitotic spindle.

Supplementary Figure S7 Mitotic defects in clathrin-depleted cells. **a**, An example of misaligned chromosomes in late mitotic figures. A clathrin-depleted HEK293 cell in telophase expressing GFP, stained for CENP-B (red) and DNA (blue). A single unsegregated chromosome (boxed region; digitally enlarged four-fold, below) is stranded between the two forming daughter nuclei. **b**,**c**, Persistent Mad2 signalling at equatorial and misaligned kinetochores in clathrin-depleted cells. Control (above) or CHC RNAi (below) cells were stained for Mad2/Cy3 (red) and CENP-B/Cy5 (blue). Cells were expressing control or CHC shRNA together with either GFP (**b**) or H2B-GFP (**c**). Scale bar, 10 μm.

Supplementary Table S1 Comparison of the main features of clathrin RNAi in rat and human cells.

72 h	Rat/siRNA		Human/shRNA	
	Control	CHC RNAi	Control	CHC RNAi
Clathrin levels	1.00 ± 0.04	0.13 ± 0.01 **	1.00 ± 0.12	0.06 ± 0.01 **
Mitotic index (%)	3.50 ± 0.20	14.20 ± 1.10 **	1.92 ± 0.21	8.42 ± 0.64 **
Misaligned chromosomes (%)	4.10 ±1.00	22.40 ± 5.40 **	9.52 ± 6.56	69.74 ± 5.84 **
Death rate (%)	0.07	0.26	1.51 ± 0.30	2.29 ± 0.51
Multiple nuclei (%)	0.50 ± 0.20	6.80 ± 1.20 **	0.77 ± 0.14	3.81 ± 0.42 **
Prometaphase interkinetochore distance (μm)	0.96 ± 0.03	0.94 ± 0.04	0.82 ± 0.02	0.84 ± 0.03
Equatorial interkinetochore distance (μm)	1.68 ± 0.06	1.55 ± 0.04	1.59 ± 0.04	1.42 ± 0.03 **

In both cell lines there was no significant difference in the death rate or in the interkinetochore distance of chromosomes not under tension. In rat cells there was no significant difference in equatorial interkinetochore distance, $p = 0.068$. Data are mean ± s.e.m. **, $p > 0.001$

Supplementary Table S2 Overview of approaches used for data shown.

	Rat cells	Human cells
Figures in main paper	Figures 1a, 1c, 1d, 2, 3a, 3b.	Figures 1b, 3c, 3d, 3e, 4, 5.
Supplementary Information	Supplementary Figures S1, S2, S3, S4, S5a-e, S6. Table 1	Supplementary Figures S5f, S7. Table 1.
Results mentioned in text	Endogenous clathrin at mitotic spindle, CME in interphase versus mitotic cells, Metaphase plate thickness	Interkinetochore distances

Supplementary Table S3 Oligonucleotides for expression of shRNA.

CHC1 sense Control shRNA	GATCCCCTCGCCCTTCTGAAGGTCCTttcaagagaAGGACCTTCAGAAGGGCGATTTTTGGAAA
CHC1 antisense Control shRNA	AGCTTTTCCAAAAATCGCCCTTCTGAAGGTCCTtctcttgaaAGGACCTTCAGAAGGGCGAGGG
CHC4 sense CHC RNAi shRNA	GATCCCCATCCAATTCGAAGACCAATttcaagagaATTGGTCTTCGAATTGGATTTTTTGGAAA
CHC4 antisense CHC RNAi shRNA	AGCTTTTCCAAAAAATCCAATTCGAAGACCAATtctcttgaaATTGGTCTTCGAATTGGATGGG

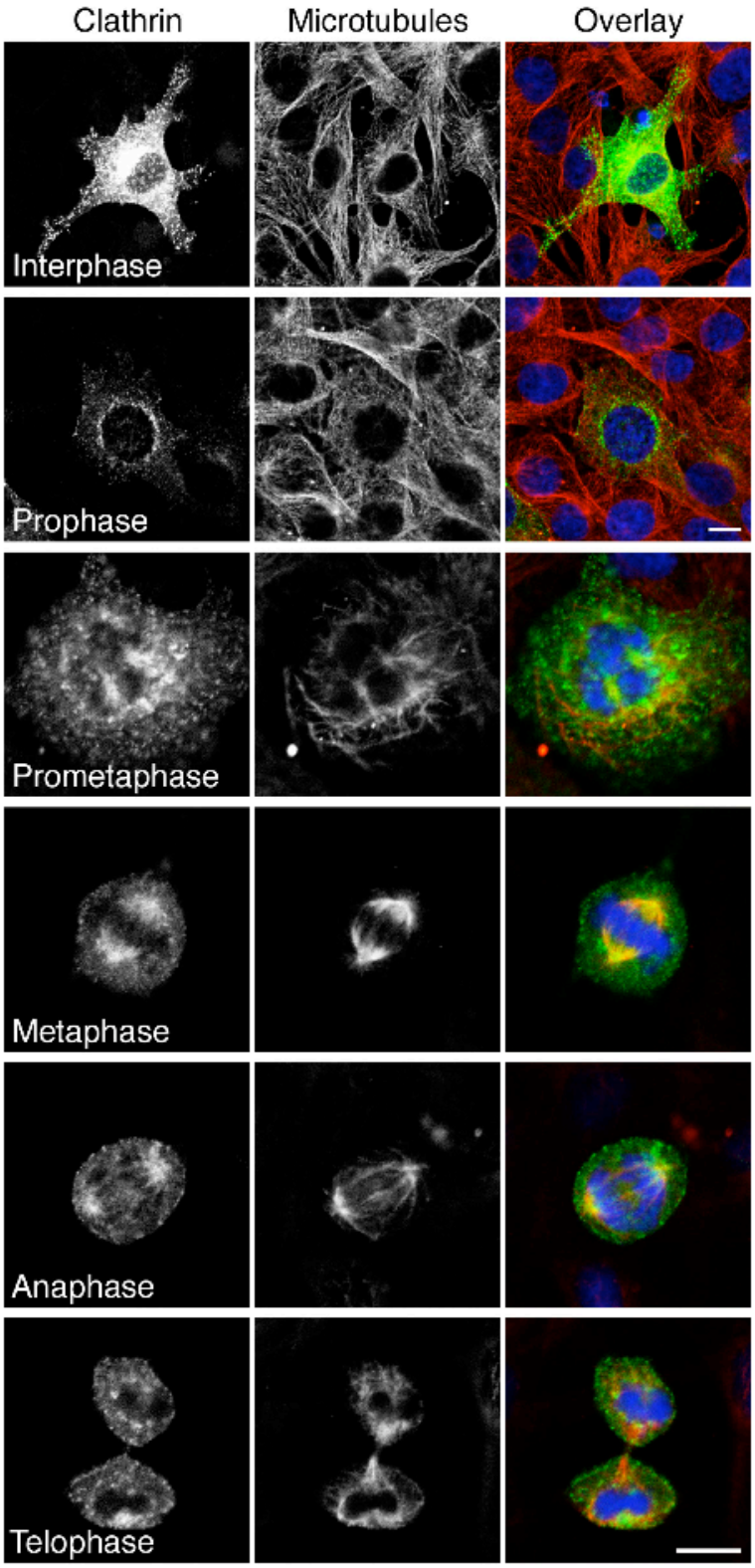
Clathrin
Microtubules
Overlay
Interphase
Prophase
Prometaphase
Metaphase
Anaphase
Telophase

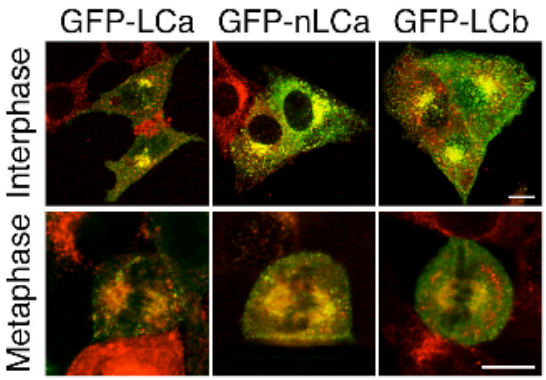
GFP-LCa
GFP-nLCa
GFP-LCb
Interphase
Metaphase

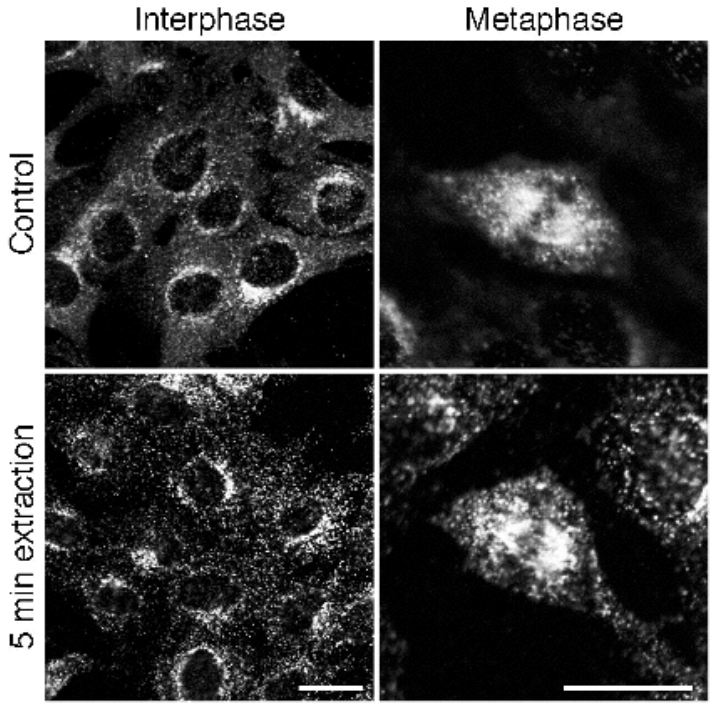
Interphase
Metaphase
Control
5 min extraction

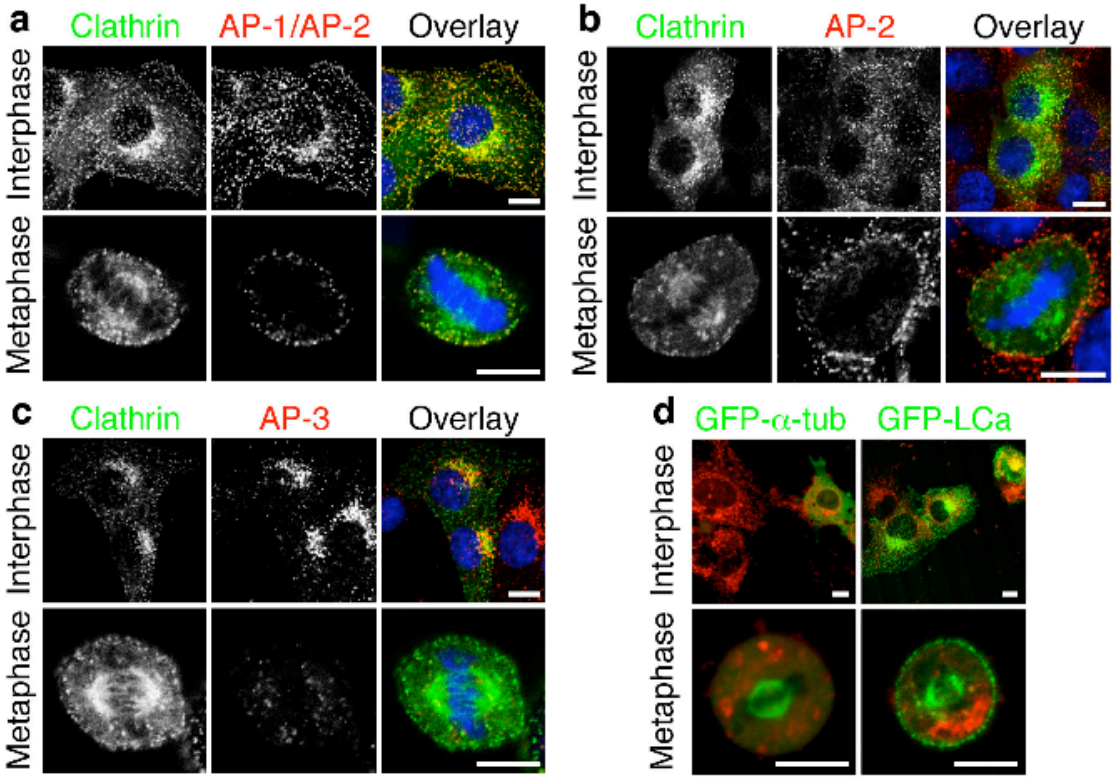
a
Clathrin
AP-1/AP-2
Overlay
Interphase
Metaphase
b
Clathrin
AP-2
Overlay
Interphase
Metaphase
c
Clathrin
AP-3
Overlay
Interphase
Metaphase
d
GFP-α-tub
GFP-LCa
Interphase
Metaphase

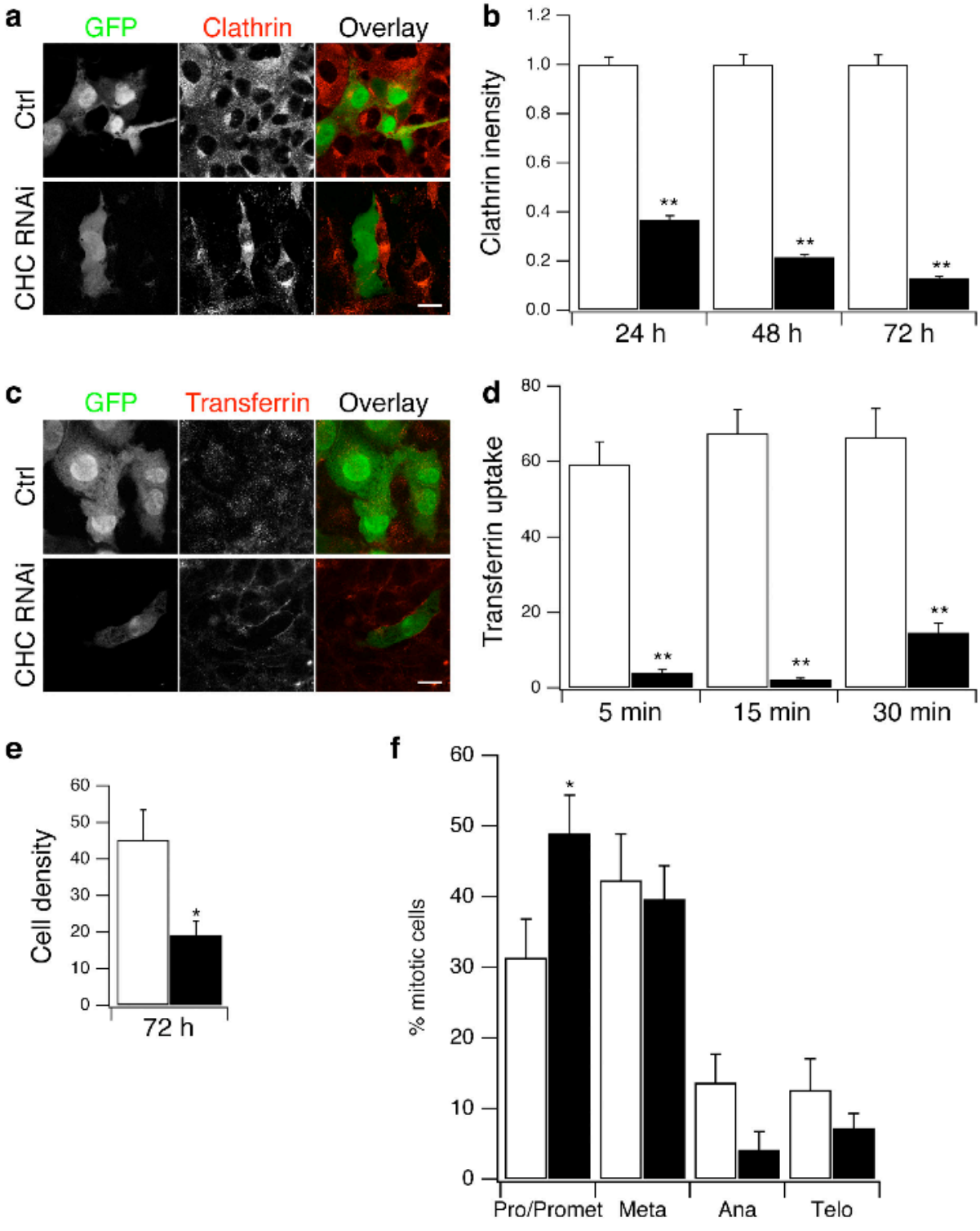
a
GFP
Clathrin
Overlay
Ctrl
CHC RNAi
b
Clathrin inensity
1.2
1.0
0.8
0.6
0.4
0.2
0.0
**
**
**
24 h
48 h
72 h
c
GFP
Transferrin
Overlay
Ctrl
CHC RNAi
d
Transferrin uptake
80
60
40
20
0
**
**
**
5 min
15 min
30 min
e
Cell density
60
50
40
30
20
10
0
*
72 h
f
% mitotic cells
60
50
40
30
20
10
0
*
Pro/Promet
Meta
Ana
Telo

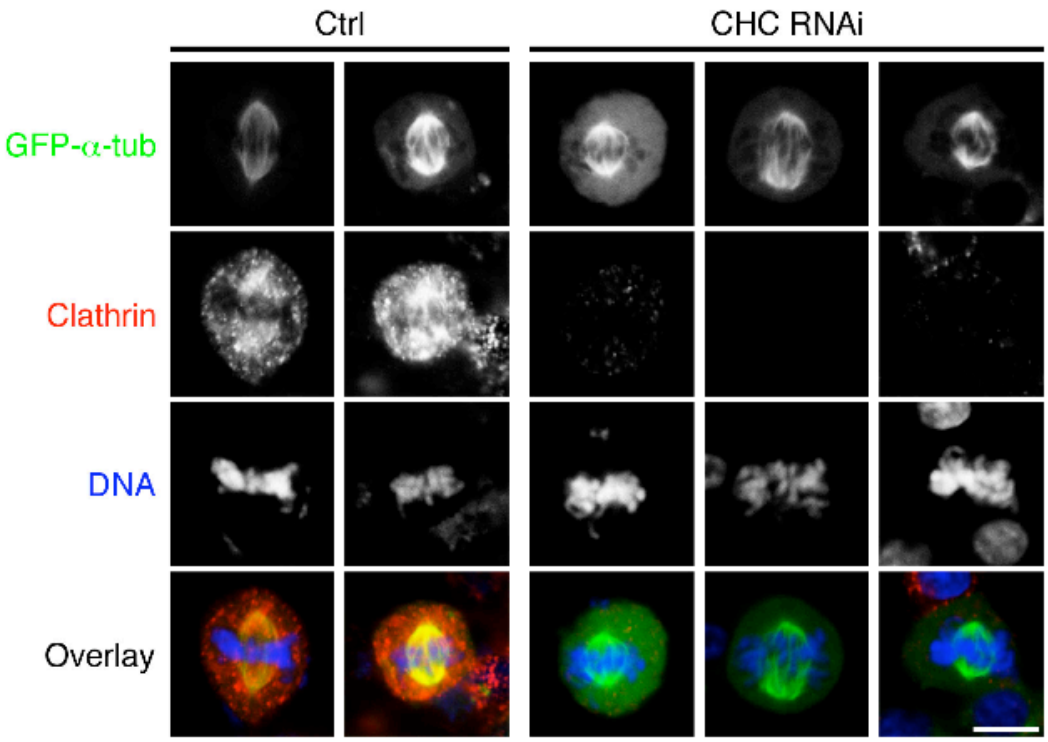
Ctrl
CHC RNAi
GFP-α-tub
Clathrin
DNA
Overlay

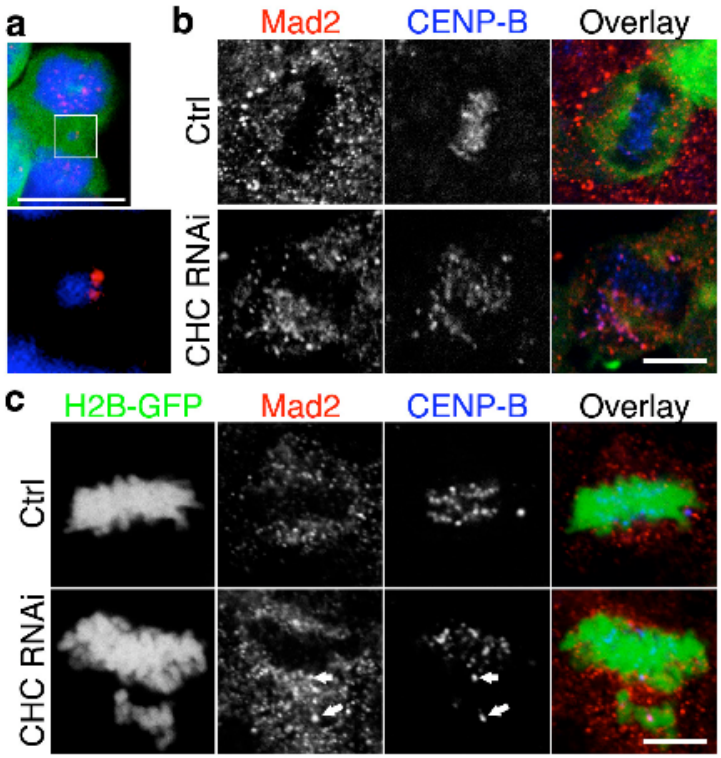
a
b
Mad2
CENP-B
Overlay
Ctrl
CHC RNAi
c
H2B-GFP
Mad2
CENP-B
Overlay
Ctrl
CHC RNAi